INTERNATIONAL JOURNAL OF CLIMATOLOGY
Int. J. Climatol. **31**: 514–530 (2011)
Published online 26 January 2010 in Wiley Online Library
(wileyonlinelibrary.com) DOI: 10.1002/joc.2090

RMetS
Royal Meteorological Society

Harmonic analysis of climatological temperature over Antarctica: present day and greenhouse warming perspectives

F. Justino,[a]* A. Setzer,[b] T. J. Bracegirdle,[c] D. Mendes,[b] A. Grimm,[d] G. Dechiche,[e] and C. E. G. R. Schaefer[a]

[a] *Universidade Federal de Viçosa, Departamento de Engenharia Agrícola, P.H.Holfs S/N, Viçosa, MG, Brazil*
[b] *Centro de Previsão de Tempo e Estudos Climáticos, INPE, Brazil*
[c] *British Antarctic Survey, High Cross, Madingley Road, Cambridge, UK*
[d] *Departamento de Física, Universidade Federal do Paraná, Curitiba, PR, Brazil*
[e] *Departamento de Ciências Atmosféricas, USP, São Paulo, Brazil*

ABSTRACT: On the basis of ERA40 and NCEP/NCAR Reanalysis (NNR) and simulations from CCCma, CCSM, CSIRO, HadCM3, MIROC-MEDRES and GFDL, which support the Intergovernmental Panel on Climate Change (IPCC) 4th Assessment Report (AR4), we demonstrated that the amplitude of the annual and the semi-annual harmonics delivered by the ERA40 and NNR is dominated by distinct seasonal variability. The maximum first harmonic amplitude of near surface temperature 2-metre air temperature (t2m) according the NNR is located over the Plateau of East Antarctica, whereas analyses for ERA40 show maximum amplitude over the west Antarctic ice sheet. The spatial pattern of the first harmonic of t2m in NNR more closely corresponds to station observations, suggesting that the seasonal cycle of t2m over Antarctica may be biased in ERA-40. A comparison between the global climate models (GCMs) and NNR demonstrates that the models satisfactorily simulate the amplitude of the first and second harmonics; however, the modelling results differ among themselves in terms of the amplitude values. Larger seasonal variability is identified for CCCma, HadCM3 and MIROC-MEDRES with values as high as 20 °C over the Antarctic plateau. We have further identified that the CSIRO GCM does not reproduce the seasonal amplitude of t2m as compared to other models, which is primarily due to its overestimation of the cloud cover and weak seasonal changes of precipitation. Calculations of the harmonic analysis based upon greenhouse warming (GW) conditions reveal that there is no substantial seasonal difference between the amplitude of the first harmonic as projected by GW and present day (PD) simulations over the Antarctic continent. Over the polar ocean, however, the amplitude of the first harmonic is reduced in all climate models under future conditions. In order to narrow down the uncertainties on future climate projections, analyses of the cloud forcing which include the short- and long-wave radiation and the surface mass balance (SMB) may provide substantial information on the cause of the discrepancies as simulated by climate models over the Antarctic region. Copyright © 2010 Royal Meteorological Society

KEY WORDS Climate changes; Antarctica; IPCC; harmonic analysis; surface temperature annual cycle

Received 27 March 2009; Revised 7 December 2009; Accepted 18 December 2009

1. Introduction

It has long been recognized that the Earth's climate is strongly linked to surface conditions in high latitudes (e.g. Bjerknes (1964), Yuan and Martinson (2000), Fyfe *et al.* (2007), Justino and Peltier (2008)). For instance, Antarctica holds 90% of the world's fresh water, and, along with its surrounding sea ice, is among the major drivers of planetary albedo dynamics. Past climate changes during the Last Glacial Maximum (LGM, approximately 21 000 years before present) were strongly affected by modifications of the thermal forcing related to enhanced ice albedo feedback, in particular during the summer season around Antarctica (e.g. Rind (1987), Justino *et al.* (2006)). Moreover, Marshall and King (1998) have found that the Southern Hemisphere (SH) reveals markedly different circulation regimes associated with extreme warm and cold Antarctic Peninsula winter temperatures.

It has been argued that the state-of-the-art global climate models (GCMs) struggle to represent the key aspects of polar climate. For instance, Monaghan *et al.* (2008) showed that 20th century annual Antarctic near-surface air temperature trends in some GCMs are about 2.5–5 times larger than that were observed. This raises questions about the robustness of the 21st century climate projections. However, Chapman and Walsh (2007) concluded that composite (11-model) GCM-simulations for 1958–2100, with forcing from historic greenhouse gas (GHG) concentrations, show warming patterns and

* Correspondence to: F. Justino, Universidade Federal de Viçosa, Departamento de Engenharia Agrícola, P.H.Holfs S/N, Viçosa, MG, Brazil. E-mail: fjustino@ufv.br

magnitudes similar to the corresponding observed trends, which are characterized by warmer conditions over the Antarctic Peninsula. GCM projections for 2001–2100, on the other hand, discontinue the pattern of strongest warming over the Antarctic Peninsula, but instead show the strongest warming over the Antarctic continent.

The different seasons provide a range of modelling challenges in the Antarctic. An assessment of errors in the simulation of the seasonal cycle may therefore help to explain inter-model differences in projections of future change. Our goal in the present paper is, therefore, to provide an additional evaluation of climate simulations from six GCMs. We focus upon the simulated seasonal cycle of surface temperature and its relationship with the atmospheric circulation over Antarctica under present day (PD) and greenhouse warming (GW) conditions. This is motivated by the fact that the model reliability in simulating PD extra-tropical climate variability will have to be carefully considered when temperature and large-scale circulation are projected for the future GW interval. Furthermore, it is important to identify possible model biases in the simulated PD Antarctic climate conditions. For analysis of future projections we have chosen GCMs simulations that are part of the Intergovernmental Panel on Climate Change 4th Assessment Report (IPCC-AR4), forced by the A2 GHG concentration scenario (SRES-A2). The SRES-A2 high emission scenarios are considered among the 'pessimist' GHG concentration scenarios.

The paper is organized as follows: Section 2 describes the climate models as well as the models implementation of the greenhouse forcing. Section 3 focuses on: (1) modelled PD mean climate and (2) inter-comparison between modelling results and the reanalyses fields for PD conditions. In addition, Section 3 explores the climate differences between GW and PD simulations. Based upon harmonic analysis (Fourier transformation), in Section 4, we evaluate the predicted seasonal cycle in terms of amplitude, phase and variance for both periods (PD and GW simulations). Section 5 summarizes our main findings.

2. Climate models

In what follows, we evaluate the climate projections for the period 2080–2100 based upon IPCC SRES-A2 GHG concentration scenario. A similar investigation focusing upon annual trends of surface temperatures has been conducted by Chapman and Walsh (2007) for the IPCC SRES-A1B scenario. The replacement of the SRES-A1B by the SRES-A2 scenario corresponds to an increase of approximately 210 ppm of CO_2 and an associated increase of global warming of up to 1 °C by 2100. The assumption of the A2 scenario may be justified by the fact that it allows us to investigate the Antarctic climate sensitivity to a substantially modified radiative forcing.

Bracegirdle *et al*. (2008) also analysed the predicted future Antarctic climate based upon a multimodel ensemble. Although the ensemble average can reduce the spread of climate projections as well as cancel out the strong biases that exist across all CMIP3 models, it does not provide a detailed individual assessment of physical reason for GCMs biases to the very challenging high latitudes of the SH. Therefore the analysis discussed here are a useful complement to the study of Miller *et al*. (2006), Chapman and Walsh (2007), Bracegirdle *et al*. (2008).

Models investigated in this study are part of the IPCC AR4 effort, and form the World Climate Research Programmes (WCRPs) Coupled Model Inter-comparison Project phase 3 (CMIP3) multimodel data set. CCCma, CSIRO, HadCM3, MIROC-MEDRES, CCSM, and the GFDL (Table I), were chosen based upon the weighting criteria proposed by Connolley and Bracegirdle (2007), in which the weighting was constructed from comparison between observation-based estimates and modelled climate according to some measure of their performance. CCCma, CSIRO, HadCM3, CCSM and GFDL have weight values among the top ten models that better reproduced the observed Antarctic climate. As previously discussed by Miller *et al*. (2006), all models contain forcing by GHG and tropospheric sulphate aerosols. While GHGs concentration is based upon measurements, sulphate forcing is calculated by offline models constrained by estimated emission of chemical precursors. Stratospheric ozone is prescribed with a seasonal cycle.

In these models, the assumption is made that during the 21st century, stratospheric ozone will slowly recover toward pre-industrial values due to the reduction of anthropogenic halogens (Miller *et al*. (2006)). The exception is CCCma where volcanic and ozone forcing are not included for both PD and GHG intervals. It should be noted that recent changes of Antarctic climate have been linked to modifications of the anthropogenic forcing associated to GHG emission, as well as to stratospheric ozone. For instance, Cai and Cowan (2007) demonstrated that climate simulations that contain time-variable

Table I. Horizontal resolution of the CMIP data utilized in this study.

Model	Country	AGCM resolution	Reference
CCCma	Canada	$3.75^\circ \times 3.75^\circ$	Flato and Boer (2001)
GFDL	USA	$2^\circ \times 2.5^\circ$	Delworth *et al*. (2006)
CCSM	USA	$1.4^\circ \times 1.4^\circ$	Meehl *et al*. (2006)
MIROC-MEDRES	Japan	$2.8^\circ \times 2.8^\circ$	Hasumi and Emori (2004)
HadCM3	UK	$2.5^\circ \times 3.75^\circ$	Pope *et al*. (2001)
CSIRO	Australia	$1.875^\circ \times 1.875^\circ$	Gordon *et al*. (2002)

stratospheric ozone forcing produced an averaged trend for the Southern Hemisphere Annular Mode (SAM) that is comparable to the trend from NNR for the late-20th century. Therefore, results presented here may be tightly related to the model treatment of the GHG forcing in particular to the coupling between the troposphere and the lower stratosphere (e.g. Kushner *et al*. (2001)).

Since the IPCC models investigated here vary in horizontal resolution (from 1.4° to 3.75°, Table I), the results presented have been interpolated to a $1^\circ \times 1^\circ$ grid by applying OACRES (Objective Analysis using the CRESsman scheme (Cressman (1959)). Multiple passes are made through the grid with increasingly smaller radii of influence. At each pass, a new value is calculated for each grid point based on a correction factor that is determined by looking at each original grid within the radius of influence. For each such grid, an error is defined as the difference between the grid value and the value from interpolation. The correction factor is based on a distance weighted formula applied to all such errors within the radius of influence. The correction factors are applied to each grid point before the next pass is made.

3. Overview of PD and GW Antarctic climates

In order to verify the GCMs capability in simulating the PD mean climate during the summer season, we compare the 2-metre air temperature (t2m) differences between the CMIP3 output and data from the European Centre for Medium Range Weather Forecasting (ECMWF) ERA40 Reanalysis as well as from the NCEP/NCAR Reanalysis (NNR, Kalnay *et al*. (1996)), over Antarctica and the Southern Ocean.

The ERA40 and the NNR data used in this study have been obtained from their data server for the period 1980–2000 (PD climatology). Near-surface temperatures over the relatively flat interior of East Antarctica are quite similar in observations and ERA40, with a small (2 °C) warm bias in winter in ERA40 (Bromwich and Fogt (2004)). However, in regions of steep orography (e.g. along coastlines and across the Transantarctic Mountains into West Antarctica), ERA40 shows biases of 5–10 °C due to errors in elevation where the resolution of ERA40 is insufficient to reproduce the real orography. Several known problems have also being identified in the NNR in Antarctica (e.g. Hines *et al*. (2000)). Chapman and Walsh (2007) by comparing NNR with surface air temperatures from land surface stations, automatic weather stations and ship/buoy observations from January to July for the years 1979–1998, show some inconsistencies between these data and the NNR. They argued that the cause of these differences may be problems in the reanalysis model's parameterization, e.g. of polar clouds and the polar boundary layer processes. However, Van den Broeke (2000) showed that from 1968 onward, the NNR is satisfactory, which includes the annual cycle of temperature, wind speed and precipitation events.

Differences are also identified by comparing the CMIP3 results with the NNR and ERA40. For brevity in what follows we provide only the comparison between the modelling results and the NNR. The CMIP3 t2m exhibits a cold bias over Antarctica of up to 10 °C for CCSM, MIROC-MEDRES and GFDL (Figure 1). The CCSM and MIROC-MEDRES t2m are lower than the NNR over Queen Mary Land (from 91.5 °E to 100.5 °E) and Wilkes Land (from 100.5 °E to 136 °E), whereas the GFDL t2m is up to 14 °C colder throughout East Antarctica. Positive anomalies are simulated by the CCCma, CSIRO and HadCM3 over the coastal region of Victoria Land in the vicinity of the Ross Sea as compared to the reanalyses. Moreover, CCCma and CSIRO models have positive t2m anomalies of 12 °C over the interior of Antarctica (Figure 1), whereas the HadCM3 in general shows anomalies between 2 and 6 °C. Therefore, the GFDL model shows the largest negative t2m anomalies over central Antarctic and the warmest climate over the Ross Sea, as compared to the reanalyses and the other GCMs. CCSM and MIROC-MEDRES, on the other hand seems to more accurately reproduce today's climate during DJF (Figure 1(b) and (e)).

For the winter season it is interesting to note the differences in the CMIP3 predicted PD climate with respect to NNR (Figure 2). While CCCma, HadCM3 and MIROC-MEDRES show negative anomalies over most of the Antarctic continent, CCSM, CSIRO and GFDL are characterized by positive and negative anomalies, although the CSIRO model shows positive values up to 14 °C (Figure 2(c)). The common feature in all CMIP3 models in JJA is the warmer conditions in the vicinity of George V Land (from 142 °E to 153.5 °E).

Over the Antarctic plateau five of the six CMIP3 models studied here show larger t2m differences compared to the NNR in winter than in summer: CCCma, CCSM, HadCM3, MIROC-MEDRES and CSIRO. Two of that five, CCSM and MIROC-MEDRES display reduced negative differences, with smaller changes in summer than in winter. This is characterized in the CCSM by the appearance of positive values (Figure 2). The HadCM3 model performs well in summer (winter) but is warmer (colder) than the NNR. Whilst CSIRO still shows larger positive differences in both seasons (Figures 1 and 2). For HadCM3, the larger negative differences to NNR dataset in winter are consistent with the fact that it simulates a low-level temperature inversion that is too strong (Turner *et al*. (2006)). Problems in simulating the low-level inversion may therefore also explain the other summer/winter contrasts mentioned above.

To further investigate the causes of t2m anomalies between the CMIP3 results and the NNR, we have evaluated the orographic features of both datasets (Fig. 3). Based on this analysis, there is no strong evidence to conclude that the t2m anomalies between these datasets are primarily associated with differences in the orography field, since the largest disagreement in the Antarctic orography as represented by CMIP results and the NNR are located around the Dome Fuji and in the Dronning Maud Land. Nevertheless, for CCSM and HadCM3 models (Figure 3(b),(d) and (f)) the positive t2m anomalies

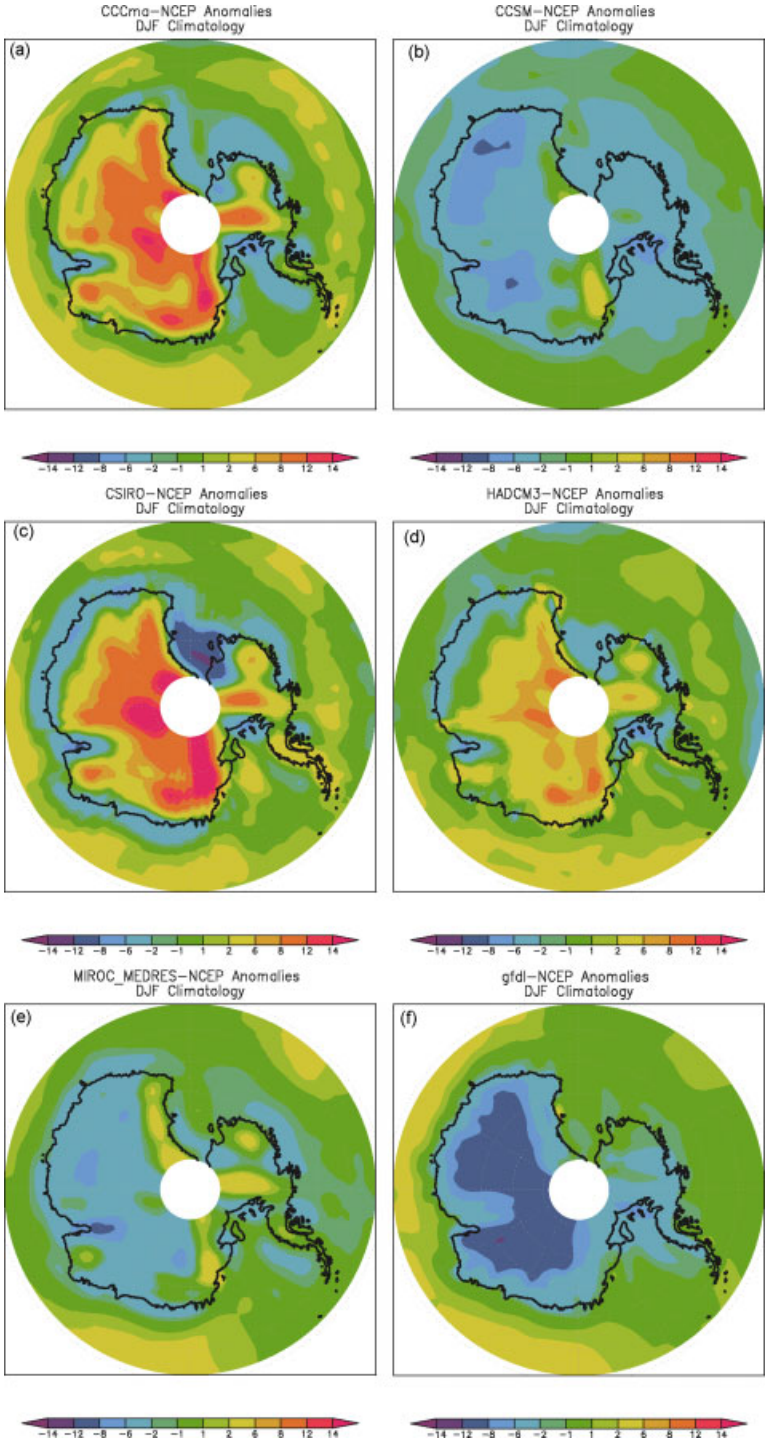

Figure 1. DJF t2m anomalies between PD simulation and NNR for (a) CCCma, (b) CCSM, (c) CSIRO, (d) HADCM3, (e) MIROC-MEDRES and (f) GFDL (°C). This figure is available in colour online at wileyonlinelibrary.com/journal/joc

over the Dronning Maud Land may be due to their lower altitude as compared to NNR and, therefore, weaker cooling effect of the atmospheric lapse rate. It may be noted that along the coast there do exist differences in the topographic features between the models and the NNR which seem to lead to t2m anomalies in particular for CSIRO and MIROC-MEDRES models, in the vicinity of Emery Ice Shelf and MacRobertson Land.

Over the oceanic areas in the Western Hemisphere during the SH winter season, the CMIP3 models are warmer than the NNR by up to 14 °C (Figure 2). One may suggest that these differences are associated with the representation of sea ice in both datasets. It may be stressed that as demonstrated by Holland and Raphael (2006), all of the models overestimate the winter sea ice variability as compared to observations. Intuitively, this would be associated with simulated colder conditions rather than higher temperatures. It is possible that the differences between CMIP3 results and the NNR is associated with stronger zonal and meridional circulations

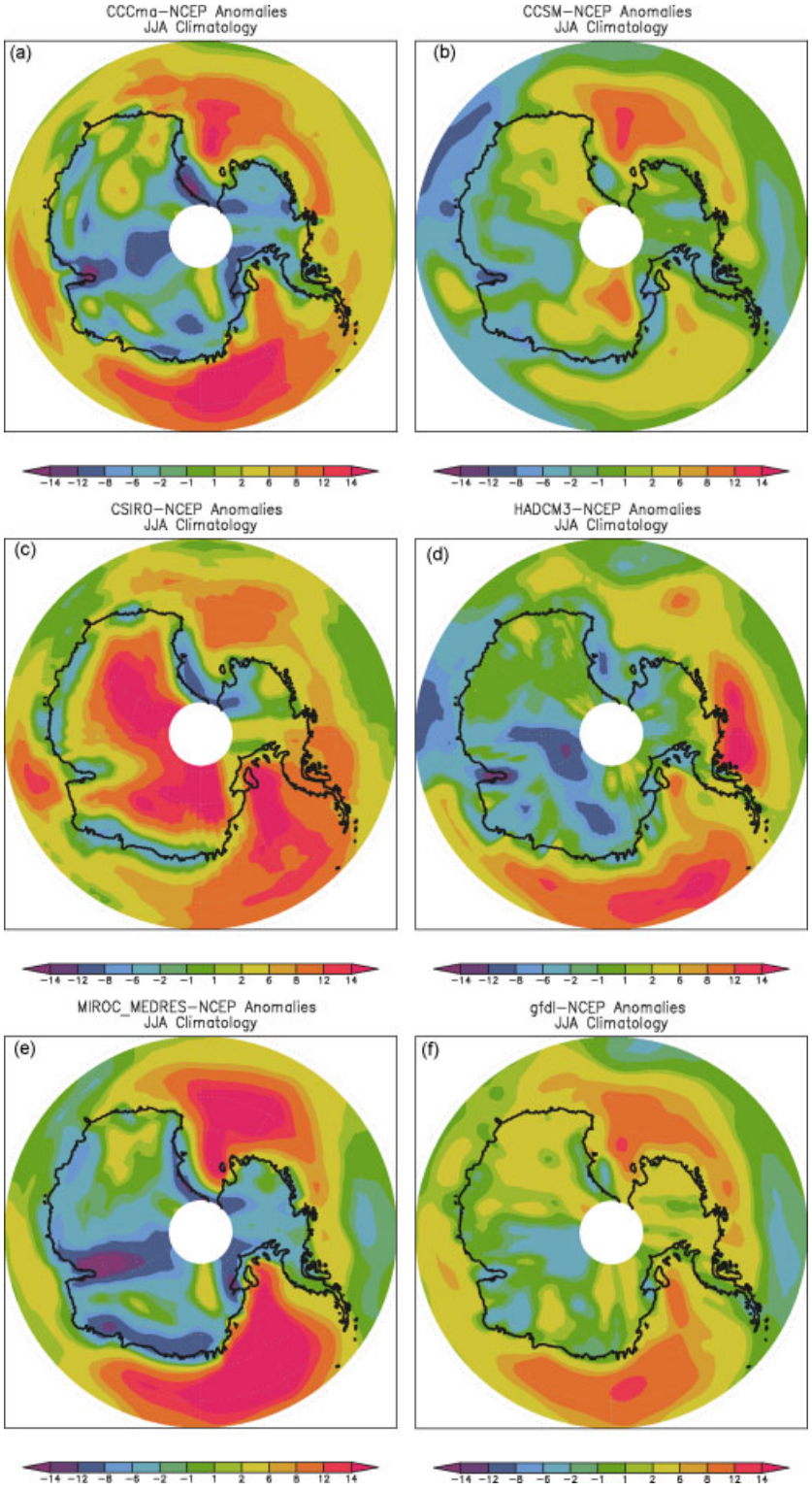

Figure 2. JJA t2m anomalies between PD simulation and NNR for (a) CCCma, (b) CCSM, (c) CSIRO, (d) HADCM3, (e) MIROC-MEDRES and (f) GFDL (°C). This figure is available in colour online at wileyonlinelibrary.com/journal/joc

as simulated by the models in respect to the NNR (not shown). This feature may induce an increase in the warm air advection from the extratropical region to the polar ocean (van den Broeke (1998), Russell *et al.* (2006)). Moreover, intensified winds invigorate the upwelling of warmer subsurface water altering the heat budget at high latitudes. Differences between the NNR and satellite and ship/buoy data in the vicinity of the Ross Ice Shelf have also been identified by Chapman and Walsh (2007).

In what follows, we evaluate the climate projections for the period 2080–2100 based upon the IPCC SRES-A2 GHG concentration scenario. Figure 4 shows the averaged DJF 2080–2100 t2m changes as projected by the CMIP3 models with respect to the averaged

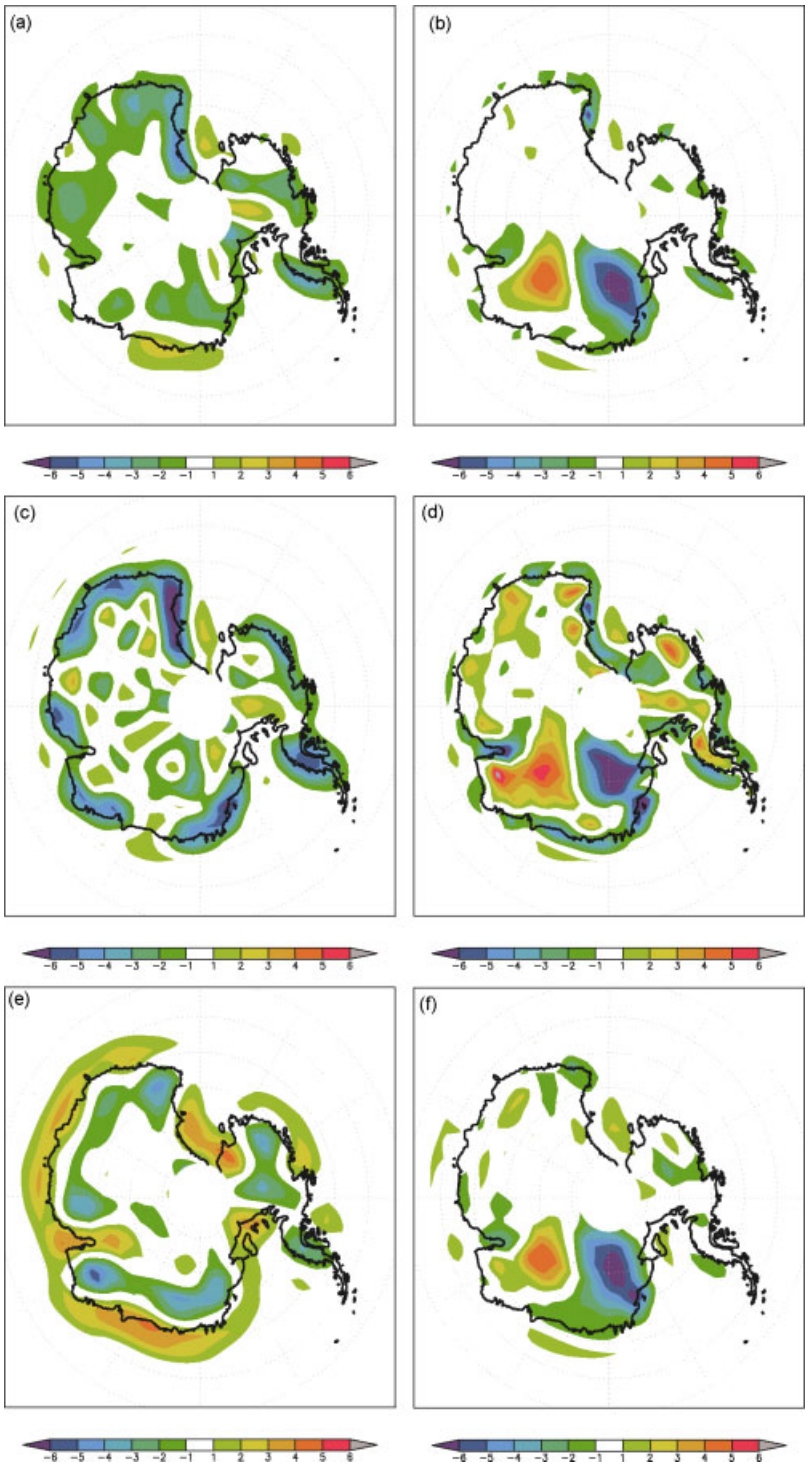

Figure 3. Anomalies between the CMIP models and the NNR topographies for (a) CCCma, (b) CCSM, (c) CSIRO, (d) HADCM3, (e) MIROC-MEDRES, (f) GFDL ($\times 10^2$ m). This figure is available in colour online at wileyonlinelibrary.com/journal/joc

1980–2000 mean climate. For summer conditions (DJF), there is generally warming over the oceanic region as well as over the Antarctic continent. The largest increases are projected by the CCSM model, which shows increases in t2m of 14 °C over land and up to 4 °C over the Southern Ocean. The continental warming as simulated in CCSM occurs over the area of intensified winds indicating the role of warmer air advection from the adjacent ocean (not shown).

A major point of concern is perhaps the inter-model differences in the spatial distribution and the magnitude of the projected changes. Although, the GCMs exhibit common features in the sense that the largest projected t2m anomalies are up to 6 °C over Central/East Antarctica (Figure 4). One may note that these temperature anomalies are tightly linked to the models' response to the radiative forcing which includes the long wave and short wave balance. Over the oceanic region the projected t2m

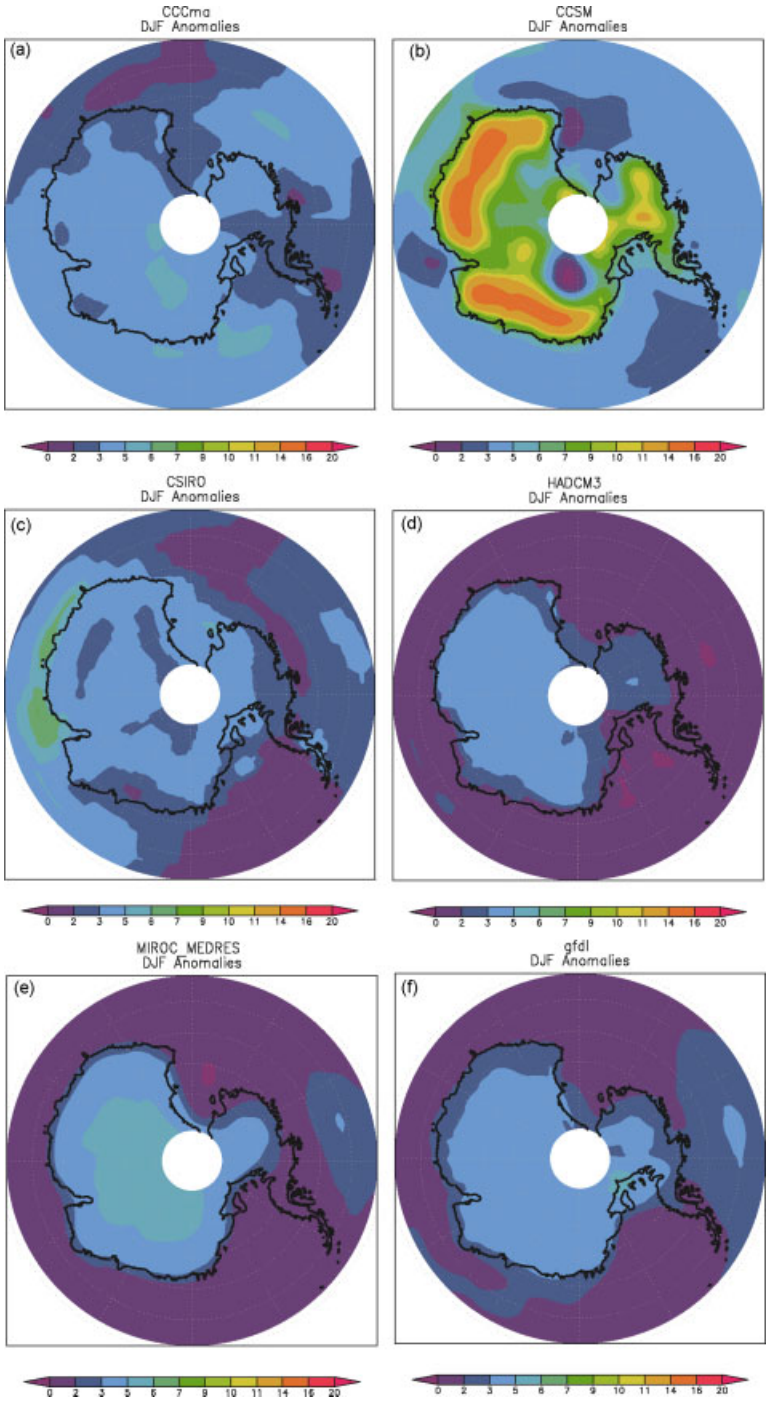

Figure 4. DJF t2m anomalies between PD and GW simulations for (a) CCCma, (b) CCSM, (c) CSIRO, (d) HADCM3, (e) MIROC-MEDRES and (f) GFDL (°C). This figure is available in colour online at wileyonlinelibrary.com/journal/joc

changes are primarily associated with the modelled sea ice distribution and the wind induced-Ekman dynamics. PD estimates of SSTs in Weddell and Ross seas during DJF vary between $\pm 2\,^{\circ}$C, thus, a 3 °C warming by the end of the 21st century as predicted by IPCC simulations will very likely inhibit sea ice formation.

Turning to JJA conditions, a remarkable warming is evident over oceanic areas for 2080–2100 as compared to 1980–2000 interval (Figure 5). The CCSM model simulates t2m anomalies as high as 20 °C over most part of the Antarctic Circumpolar Current (ACC), the other models (CCCma, CSIRO, HADCM3, MIROC-MEDRES and GFDL) are associated to weaker t2m anomalies. Despite differences in the t2m response to GW conditions there are similarities among the models. For instance, CCCma and CSIRO are characterized by higher t2m anomalies over East Antarctica whereas MIROC-MEDRES and GFDL are dominated by t2m anomalies mainly placed in West Antarctica. The larger t2m changes occur primarily in areas of deep water formation, namely in the Ross/Bellingshausen and Weddell seas (Figure 5).

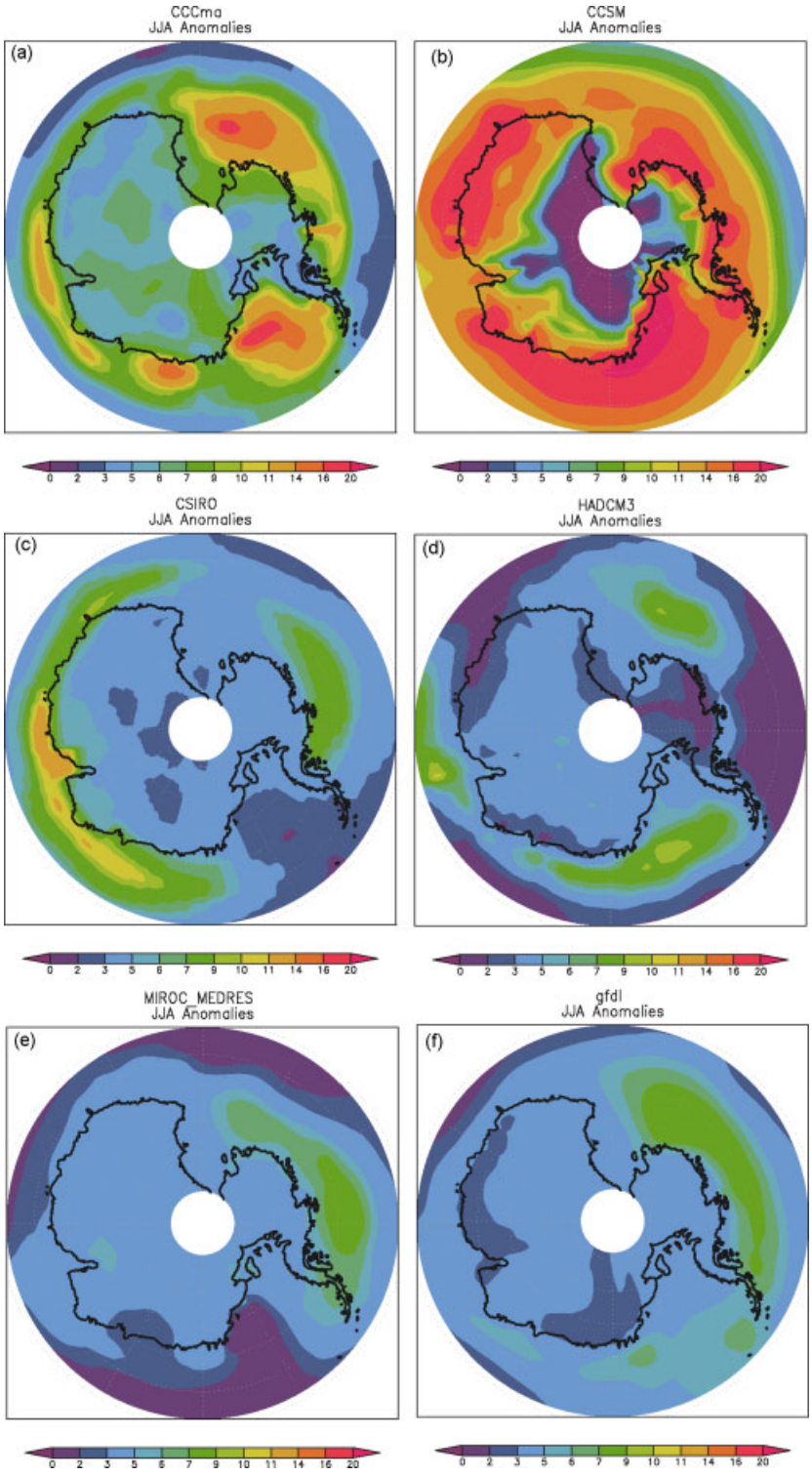

Figure 5. JJA t2m anomalies between PD and GW simulations for (a) CCCma, (b) CCSM, (c) CSIRO, (d) HADCM3, (e) MIROC-MEDRES and (f) GFDL (°C). This figure is available in colour online at wileyonlinelibrary.com/journal/joc

The CCCma and HadCM3 show a close link between the t2m anomalies and the magnitude of surface wind anomalies (not shown). It is found that the areas with more vigorous wind in the GW simulation as compared to PD conditions also exhibit higher near-surface temperature changes. Although the magnitude of the wind field changes as simulated by these two models does not strongly differ from those predicted by the other models (0.8–1.4 m/s). These projected changes in t2m may still allow sea ice formation in the future, since these regions in the winter season under today's conditions typically experience values between −21 and −30 °C. One would expect, however, a reduction in sea ice thickness as detected by Lefebvre *et al.* (2004). Reduction in the sea ice thickness is associated with modification in the atmosphere–ocean heat transfer and consequently might

be associated with anomalous maritime air advection and perhaps enhanced warming over the coastal areas. Figure 5 shows, furthermore, that the remarkable local maximum warming tendency over the Antarctic Peninsula, as it has been observed in the last 30 years, is absent in the future climate projections.

4. Harmonic analysis

4.1. PD and GW climates

In order to study the seasonal spatial variability of t2m we have applied harmonic analyses. As discussed by Aslan *et al*. (1997), the Fourier transformation or harmonic analysis decomposes a time-dependent periodic phenomenon into a series of sinusoidal functions, each defined by unique amplitude and phase values. The proportion of variance in the original time-series dataset accounted for by each term of the harmonic analysis can also be calculated (Jakubauskas *et al*. (2001)).

The first order harmonics of meteorological parameters show long-term effects, while higher order harmonics show the effects of short-term fluctuations. The phase angle can be used to determine the time when the maximum or minimum of a given harmonic occurs. The harmonic analysis is, therefore, a useful tool to characterize different climate regimes and transition regions. Moreover, the advantage of using this mathematical approach is associated with the possibility of identifying dominant climate features in the space–time domain. One may note that investigations based upon area averaged time series are embedded with small and large-scale processes dictated by distinct periodicity, this in turn may cancel out these regional climatic signals in the space–time domain. Harmonic analysis is based on the series of trigonometric functions (Wilks (1995)), as described below:

$$y_t = \overline{y} + \sum_{j=1}^{N} C_j \cos(\omega_j t - \varphi_j)$$

y_t is the value at time t, $\overline{y}$ stands for the arithmetic mean, C_j is the amplitude of harmonics, t the time, ω_j is the frequency and ϕ_j is the phase angle, and N represents the number of observations. The amplitude is calculated from

$$C_j = \sqrt{A_j^2 + B_j^2}$$

In which A_j and B_j are given by:

$$A_j = \frac{2}{N}\sum_{t=1}^{N} y_t \cos\left(\frac{2\pi t}{N}\right); \quad B_j = \frac{2}{N}\sum_{t=1}^{N} y_t \sin\left(\frac{2\pi t}{N}\right)$$

The phase angle is dependent on A_j value and may be computed as follows:

$$\varphi_j = \begin{cases} \tan^{-1}\dfrac{B_j}{A_j} \mathrm{A}_j > 0 \\ \tan^{-1}\dfrac{B_j}{A_j} \pm \pi \text{ or } \pm 180^{\circ} \mathrm{A}_j < 0 \\ \dfrac{\pi}{2} \text{ or } 90^{\circ} \mathrm{A}_j = 0. \end{cases}$$

Contribution by individual harmonics (j) to total variance of the timeseries is given by $j = \dfrac{C_j^2}{2s^2}$, where s is the timeseries variance.

The potential of the harmonic analysis approach in the classification of eco-climatic zones has been discussed by Azzali and Menenti (2001). It has also been demonstrated that fundamental characteristics related to the inter- and intra-seasonal characteristics of dynamic ecosystems, may be identified by harmonic analysis. Several studies have focussed on the semi-annual harmonic due to its climate linkage with distinct climate modes, such as the Southern Annular Mode (SAM), quasi-stationary wave-3 pattern (ZW3) and the Pacific South American pattern (PSA) (e.g. Yuan and Li (2008)). During the last four decades several studies have explored the use of harmonic analysis to characterize the SH polar climate. van Loon (1967) utilized harmonic analysis and found that the temperature contrast between middle and polar latitudes in the SH is linked to increased cyclonic activity in high latitudes over the Antarctic Ocean, where the second harmonic of the mid-tropospheric meridional temperature gradient has a magnitude exceeding that of the first harmonic. This led to the identification of the semi-annual oscillation (SAO) at middle and high southern latitudes. Meehl (1991) further investigating the SAO, argued that along with the observed upper-ocean temperature profiles, changes in the annual cycle of SST and ocean heat storage near 50 °S could lead to a modulation of the observed SAO. Furthermore, it has been found that changes in Antarctic temperature may be influenced by the SAO as a result of the amplification of the wave-3 structure of the atmospheric circulation (van den Broeke (1998), Raphael and Holland (2006)).

Figure 6(a) shows the amplitude of the first harmonic of t2m based upon the ERA40 and NNR datasets. This harmonic explains at least 88% of the variance of the timeseries of t2m in the Antarctic region for both datasets. However, for the ERA40 this harmonic shows smaller variance south of 80 °S. The first harmonic of t2m according to the ERA40 Reanalysis is primarily characterized by a tripolar structure over the continent around the South Pole. Over East Antarctica, the two nodes of variability are influenced by the highest parts of Antarctica.

A different picture is seen in the NNR data, in the sense that the largest seasonal variability is located over the Weddell and Ross seas and over the highest topographic features (Dome Fuji and Dome C). The ERA40 and NNR reanalyses also differ with regard to the amplitude values, i.e. the NNR data shows a stronger seasonal contrast (Figure 6(a) and (c)). It should be noted that differences are also identified over the coastal region over East Antarctica where the ERA40 exhibits reduced seasonal contrast. According to Monaghan and Bromwich (2008), snowfall and surface temperature variability are tightly correlated in higher elevation regions, therefore, it is possible that the seasonal changes of snowfall through changes of the radiative balance may feedback

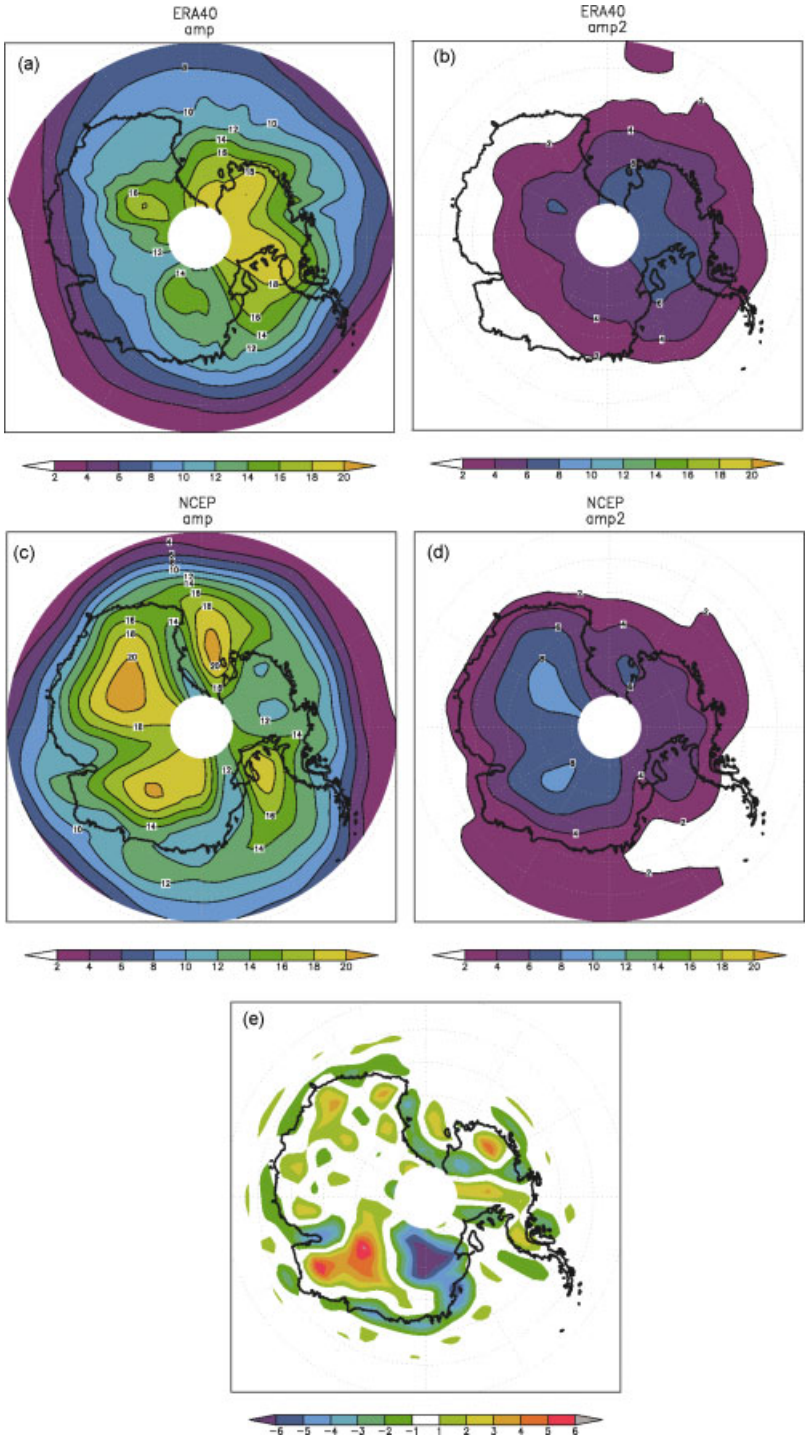

Figure 6. Amplitude of the first harmonic of t2m for ERA40 Reanalysis. (a, b) is the amplitude of the second harmonic. (c, d) is the same but for the NNR. (e) is the orography anomalies ($\times 10^2$ m) between the NNR and ERA40 Reanalyses (°C). This figure is available in colour online at wileyonlinelibrary.com/journal/joc

to modify the surface temperature, both upstream and downstream of the topographic features. Moreover, van den Broeke *et al*. (2005) argue that regions with a steep slope force seasonal katabatic winds that mix relatively warm air downward to the surface, which results in higher temperature and consequently induces a strong seasonal contrast.

Over the ACC region the amplitude of the first harmonic is less than half of the maximum over the Antarctic continent. However, the seas adjacent to West Antarctica, which include the Ross and Weddell seas, are dominated by a larger amplitude of the first harmonic (Figure 6(a) and (c)), in particular for the NNR dataset. This is probably associated with seasonal changes of sea ice which induce modifications in the radiative budget (King (1994)), and can affect the thermal advection onto the ice shelves. Additionally, the absence of katabatic winds in these areas allows for the generation of a

temperature inversion in winter at the surface enhancing the seasonal contrast. By assuming that the first two harmonics explains more than 90% of the total variance of the t2m, the amplitude maxima over the Ross and Weddell seas has also been identified by van den Broeke (1998), for Halley and Belgrano stations in the area of the Weddell Sea, and for Hallett and Little America in the Ross Sea.

Figure 6(e) shows differences in the topography height between the NNR and the ERA40 reanalyses. The NNR is characterized by higher (lower) altitude in the east side (west) of the Dome Fuji than the ERA40 dataset. Moreover, differences are noted between both data in the Dome C and in the George V Land. These areas show the large disagreement between the NNR and the ERA40 in terms of their annual and semi-annual harmonics (Figure 6). It is therefore very likely that the enhanced seasonal contrast of the t2m in the NNR is due to stronger annual forcing of the katabatic winds compared to ERA40.

Turning to the second (semi-annual) harmonic, one may note that the areas with larger amplitude values are very similar to those seen in the annual harmonic. As detected for the first harmonic, higher amplitude values are found over Antarctic plateau for the NNR and over the West Antarctica ice sheet for the ERA40 dataset. By comparing our results with the semi-annual harmonic based on station data, one may note that the NNR reproduces the observed data satisfactorily, since the higher amplitude is observed in the Vostok, Dome C and Plateau station. This feature is primarily linked to the magnitude of the temperature inversion in winter associated with the loss of long wave radiation.

van den Broeke (1998) evaluating the influence of the SAO on near-surface temperatures in Antarctica, found that the variance explained by the second harmonic of the annual temperature cycle is largest on the Antarctic Plateau (11–18%), followed by the large ice shelves and coastal East Antarctica (6–12%) and stations at or close to the Peninsula (0–5%). These results match the explained variance seen in the NNR and the ERA40 over the Antarctic Plateau, but they disagree with regard to the variance over East Antarctica and Peninsula in ERA40. A comparison between the CMIP3 results and the Reanalysis data (Figure 7) clearly demonstrates that the models can satisfactorily simulate the amplitude of the first harmonic, as well as its spatial pattern as reproduced by the NNR. The CMIP3 results are primarily characterized by the topographic effects over regions such as the East Antarctica Ice Sheet (EAIS, Figures 6 and 7). The second region with higher amplitude values is located over the Ross and Weddell seas. Comparison between the CMIP3 models and the ERA40 reveals a disagreement on the areas of higher seasonal harmonic variability. This may indicate a bias in the ERA40 dataset with regard to the amplitude of the seasonal cycle. Studies of Antarctic climatology show that the largest seasonal amplitude of temperature variation is found over the high plateau, not over the relatively low-lying West Antarctica (Warren (1996), Broeke *et al*. (2005)).

It should be noted that despite having reasonable horizontal resolution, the CSIRO model (Table I) did not exhibit the seasonal variability as predicted to occur by the other models, as well as by the Reanalysis. One may argue that this feature could be associated with a bias in the model's representation of the wave 3 pattern (ZW3, van den Broeke (1998)). However, it has been shown by Raphael and Holland (2006) that the CSIRO model does a respectable job of simulating ZW3 spatially. This anomalous amplitude as predicted to occur by the CSIRO model is perhaps consequence of processes linked to the cloud cover, or may be associated with the treatment of the ice/snow subsurface temperature and heat flux. Phipps (2006) evaluating the CSIRO Mk3L climate system model, a simplified version of the CSIRO model evaluated here, shows that the model can be seen to have excessive cloud cover south of 60 °S as compared to NCEP-DOE Reanalysis.

To further evaluate the discrepancies in simulating the seasonal changes in the CMIP3 models, we show in Figure 8 the annually zonally averaged total cloud cover (TCC) over the SH ocean and Antarctica, and the annual march of the TCC averaged between 87 °S–70 °S and 30 °E–130 °E. It may be demonstrated that the GFDL and CSIRO models show the largest values of the TCC compared to the other models (Figure (a)). This overestimation of clouds may very likely damp the annual cycle of temperature, as reproduced by the CSIRO and GFDL models. It is interesting to note, moreover, that the models differ substantially in terms of the seasonal cycle of the TCC over the Antarctic Plateau (Figure 8(b)). This may be the cause of the inter-model differences in amplitude of the t2m annual harmonic. Again, larger seasonal variability of t2m is identified for CCCma, HadCM3 and MIROC-MEDRES with values as high as 20 °C. It should be mentioned that these model results fit closely with the NNR dataset (Figures 7 and 6). The larger amplitude of the annual harmonic over seasonally ice covered regions in the CMIP3 models and the NNR, may be due to modifications in the heat flux exchange between ocean and atmosphere linked to the seasonal sea ice melting. Additionally, as proposed by Broeke *et al*. (2005), the amplitude of the annual cycle of t2m over coastal regions is also caused by the nonlinear response of air moisture content, clear-sky conditions and the long wave radiation balance.

Over the Antarctic continent the explanation for strong seasonality is not straightforward. Previous investigations based upon the Antarctic surface mass balance (SMB), for which precipitation (P) minus sublimation (E) is an important parameter, demonstrate that the minimum value of P-E is located over the Plateau of East Antarctica (Vaughan *et al*. (1999)). This analysis matches very closely to our identified area of maximum first (or annual) harmonic amplitude of t2m, as shown in Figure 7. It has been demonstrated moreover that the SMB is affected by the amount of clear-sky precipitation as proposed

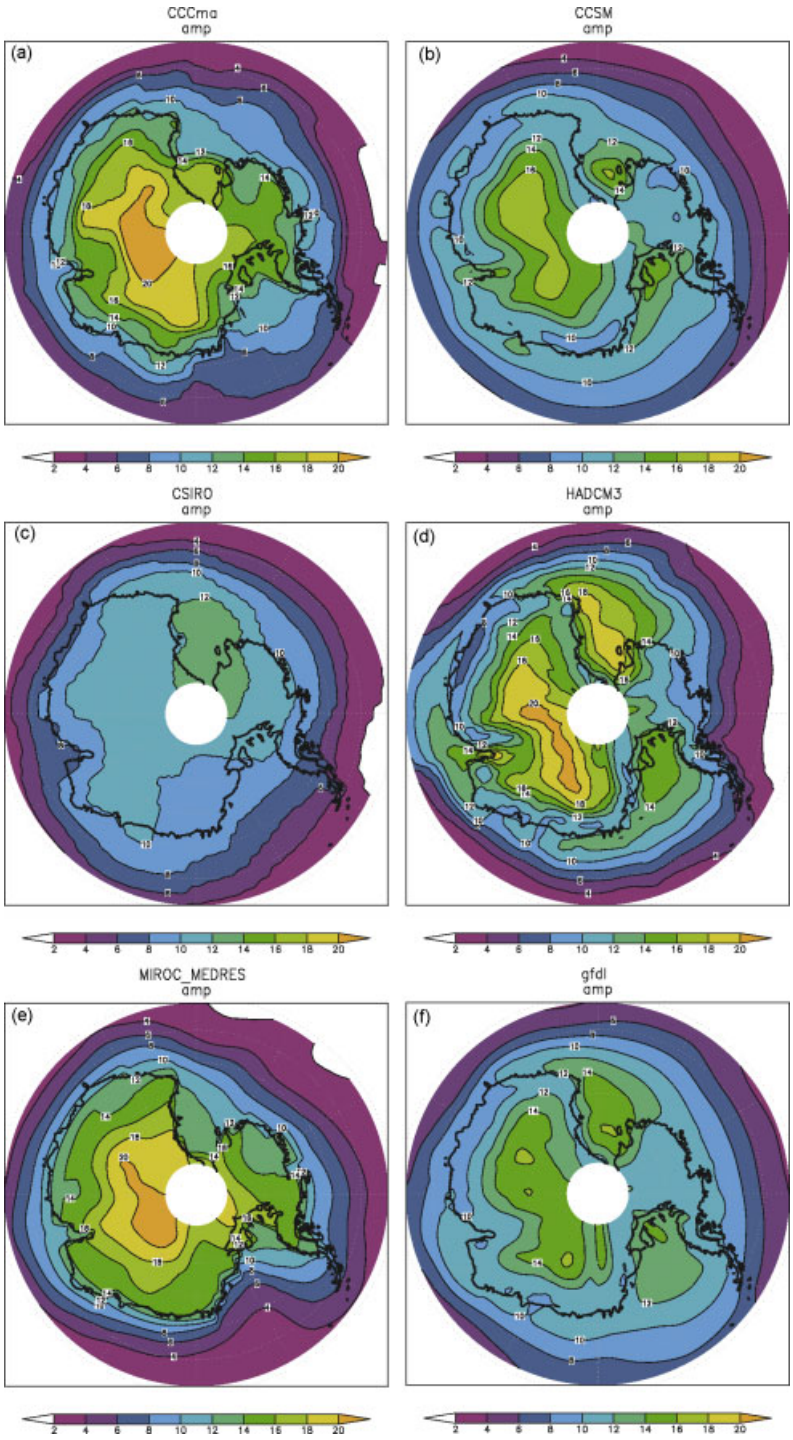

Figure 7. Amplitude of the first harmonic of t2m for (a) CCCma, (b) CCSM, (c) CSIRO, (d) HadCM3, (e) MIROC-MEDRES and (f) GFDL (°C). This figure is available in colour online at wileyonlinelibrary.com/journal/joc

by Cassano *et al.* (2001). Based on precipitation which may be used as a proxy for the SMB (not shown), it is demonstrated that the CSIRO model does not reproduce the seasonal cycle of precipitation and also overestimates the TCC throughout the year, as previously mentioned (Figure 8(a) and (b)). On the other hand, models with higher seasonal variability of t2m are associated with small TCC amount and reasonable representation of the annual cycle of precipitation. One may argue, therefore, that the simulated amplitude of the annual cycle of t2m in the interior of Antarctic, may very likely be associated with the model treatment of the P-E rate. This involves the cloud-forced short wave and long wave radiation (up and down) balance.

Analyses of the semi-annual harmonic amplitude of t2m (Figure 9), show that the largest intra-seasonal variability is located over the EAIS with values as high as 8 °C according to the HadCM3 and MIROC-MEDRES output. Small values are simulated by CCCma and GFDL models. In addition, the second harmonic

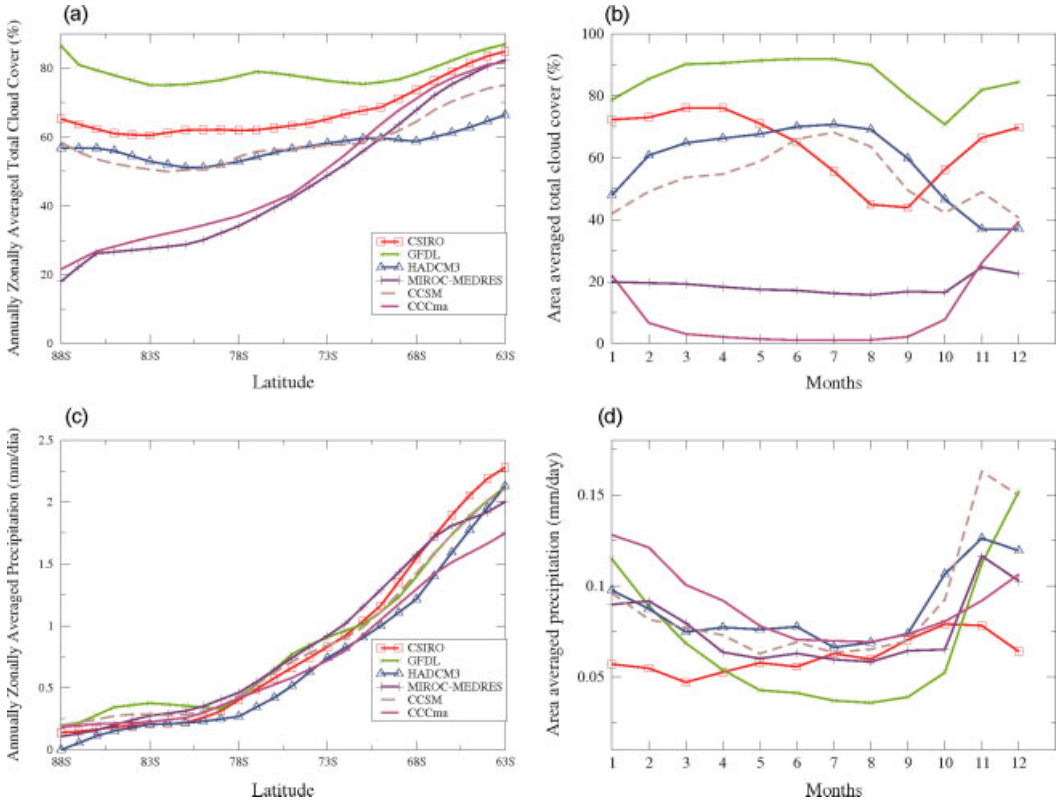

Figure 8. (a)Annually zonally averaged total cloud cover (%) and (b) area-averaged total cloud cover over 87 °S–70 °S and 30 °E–130 °E (%). This figure is available in colour online at wileyonlinelibrary.com/journal/joc

of the CMIP3 data shows a very similar spatial pattern to the NNR, except for the CSIRO model. The CMIP3 results also exhibit a higher amplitude over the Ross and Weddell seas, as found by van den Broeke (1998), which characterizes the intra-seasonal behaviour of the coupling between the sea ice and the atmospheric circulation. It should be emphasized that CCCma and CSIRO differ from the other models along the coastal region of East Antarctica. It has been demonstrated that the second harmonic of t2m is highly correlated with the second harmonic of pressure (SAO), due to the displacement of the low pressure belt during the distinct phases of the SAO (van den Broeke (1998)). Based on this, one may suggest that the linkage between the ZW3/SAO patterns with the near-surface temperature variability is inadequately simulated in CCCma and CSIRO models.

Calculations of the harmonic analysis based upon GW conditions reveal that global warming affects the annual cycle of Antarctic temperature in different ways over the ocean and the continent (Figure 10). In the interior of the Antarctic continent, there is no substantial seasonal difference between the amplitude of the first harmonic as projected by GW and PD simulations, with values between $\pm 1\,^{\circ}$C. Over the ocean along the ACC the amplitude of the first harmonic is reduced in all IPCC models in the GW interval compared to the PD interval (Figure 10). The CMIP3 models show large weakening of the annual cycle over the Pacific and Atlantic sectors except for the MIROC-MEDRES. This weakening in the amplitude of the first harmonic is due to higher winter temperatures which is associated with reduced sea ice thickness and sea ice area (not shown). The CCSM model, however, shows a strengthening in the amplitude of the first harmonic in the interior of the Antarctic continent (Figure 10(b)), which is primarily a result of increased temperature during the summer season (see Figure 4). In addition, over the ACC the CCSM exhibits the largest changes in the amplitude of the seasonal cycle between the PD and GW simulations (Figure 10(b)).

An analysis of the difference in the amplitude of the first harmonic of near-surface wind (not shown), between the GW and PD intervals does not reveals a clear relationship with the temperature changes discussed here. Lefebvre *et al*. (2004) argued that the CCSM model overestimates the sea ice area under PD conditions in particular in the Pacific and the Indian sectors. This anomalous pattern induces very cold conditions in winter due to the isolation of the atmosphere from the underlying warm ocean. Turning to GW conditions, the opposite is verified with increased temperature as a consequence of strongly reduction in the sea ice cover, which allows a more effective heat exchange between the ocean and the atmosphere (Figure 5(b)). Concomitantly, this is associated with a reduction of the amplitude of the annual harmonic.

Since changes of the amplitude of the second harmonic as projected by the climate simulations between the two epochs are relatively small, they are not shown here. It should be noted that larger changes occur over the oceanic areas along the ACC, in particular over

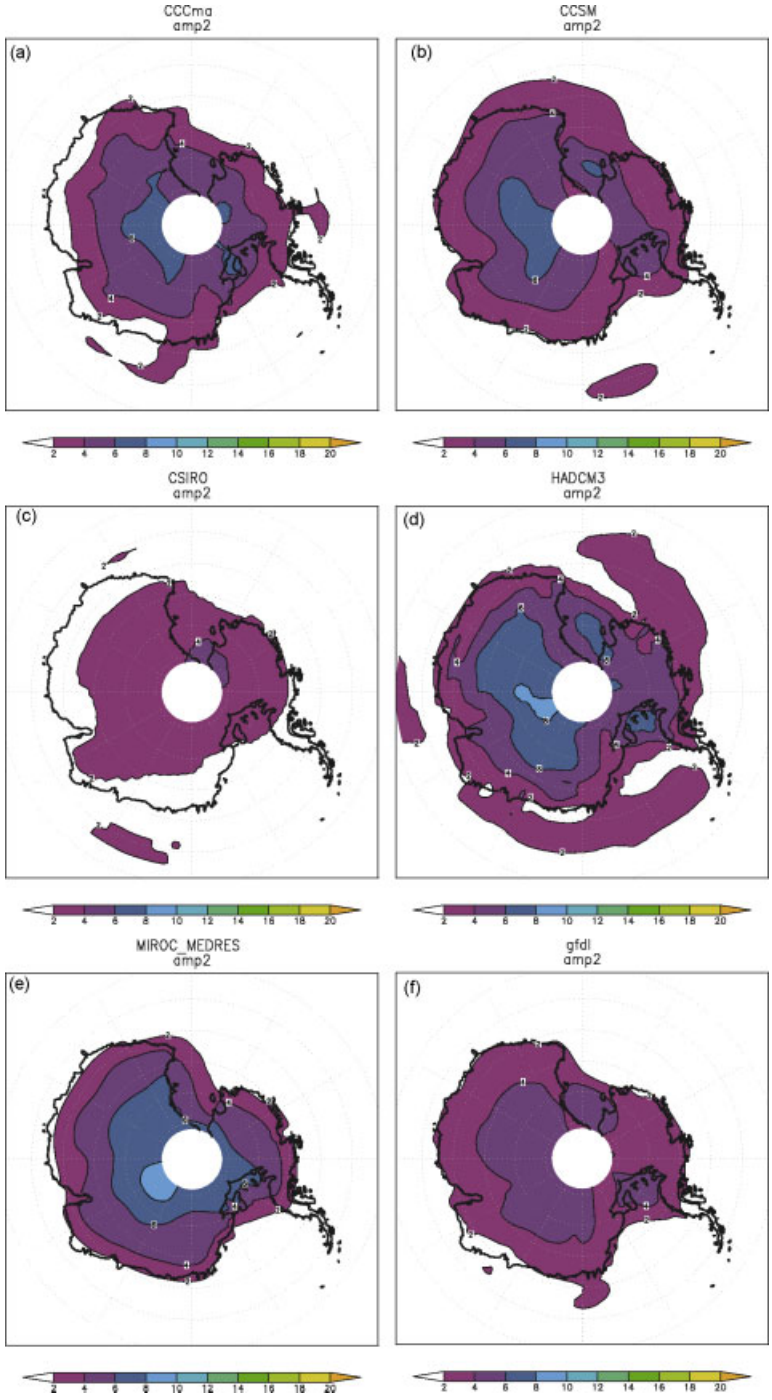

Figure 9. Amplitude of the second harmonic of t2m for (a) CCCma, (b) CCSM, (c) CSIRO, (d) HadCM3, (e) MIROC-MEDRES and (f) GFDL (°C). This figure is available in colour online at wileyonlinelibrary.com/journal/joc

Weddell and Ross Seas. This highlights the importance of sea ice in driving the annual cycle of the near-surface temperature in the SH polar region. Over the continent, a strengthening of the semi-annual cycle under GW conditions is seen in the CCSM model results.

5. Conclusions

Based on the ERA40 and NNR Reanalyses, and climate simulations from six GCMs (CCCma, CCSM, CSIRO, HadCM3, MIROC-MEDRES and GFDL), that support the IPCC AR4, we have provided an investigation of the simulated near-surface temperature over the SH polar region, with a particular emphasis on the amplitude of the annual and semi-annual cycle. Our focus include both PD and GW conditions.

It has been demonstrated that there are several differences between the CMIP3 PD simulations and the NNR. These differences are larger over the Antarctic continent in the summer season, where the modelled t2m is up to 10 °C higher than the NNR for CCSM, MIROC-MEDRES and GFDL. On the other hand, the CCSM

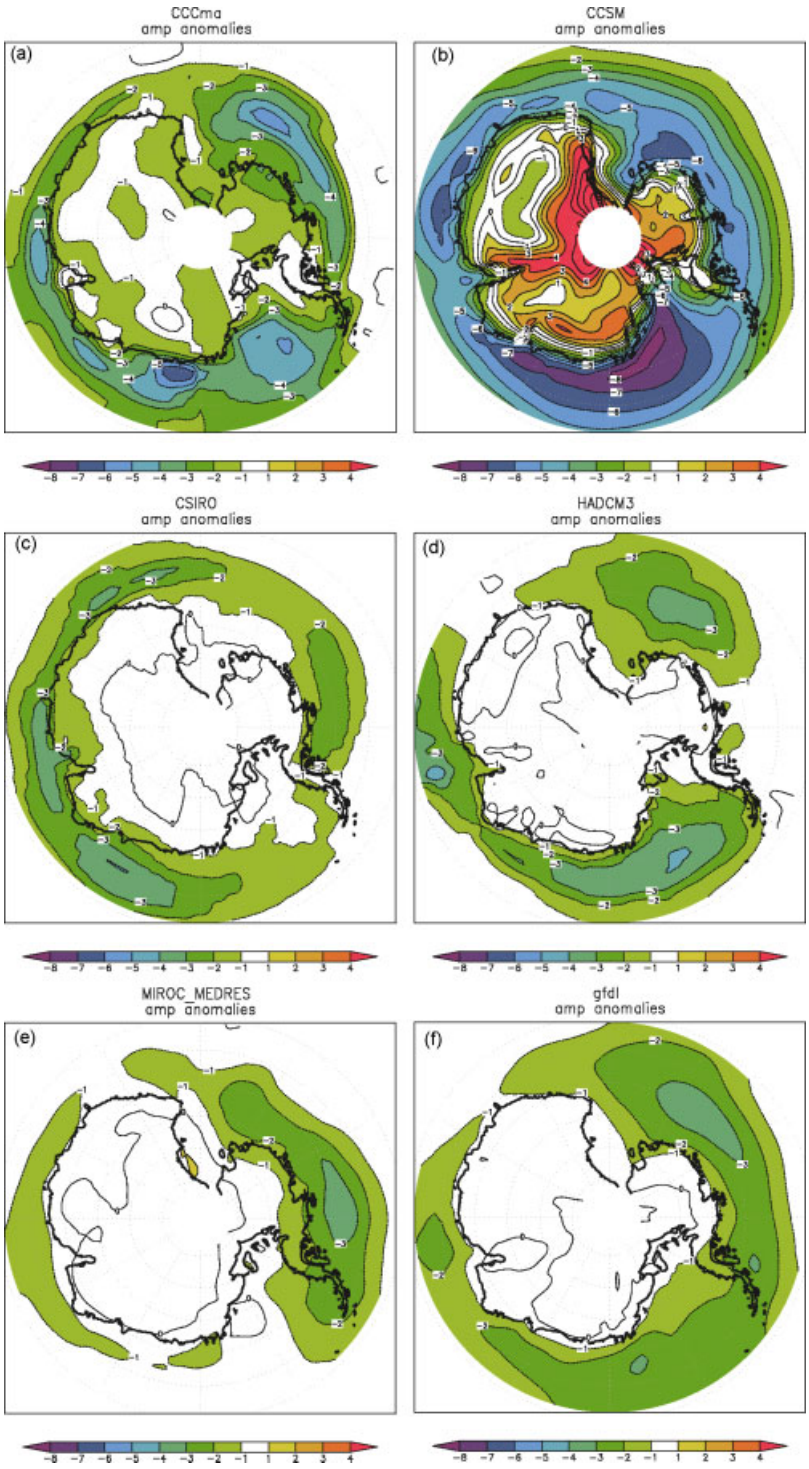

Figure 10. Amplitude anomalies of the first harmonic of t2m between PD and GW simulations for (a) CCCma, (b) CCSM, (c) CSIRO, (d) HadCM3, (e) MIROC-MEDRES and (f) GFDL (°C). This figure is available in colour online at wileyonlinelibrary.com/journal/joc

and MIROC-MEDRES t2m are lower than the NNR over Queen Mary land and Wilkes land, whereas the GFDL t2m is up to 14 °C colder throughout East Antarctica. In winter, while CCCma, HadCM3 and MIROC-MEDRES show negative anomalies over the majority of the Antarctic continent, CCSM, CSIRO and GFDL are characterized by positive and negative anomalies. Analyses of the orographic features of both datasets (Figure 3) do not reveal strong evidence to conclude that these t2m anomalies between the CMIP3 and the NNR are primarily associated with differences in the orography field, since the largest disagreement in the Antarctic orography as represented by CMIP results and the NNR are located around the Dome Fuji and in the Dronning Maud Land. Although, it may be noted that along the coastline there are differences in topography between the models and the NNR, which seem to lead to t2m anomalies in particular for CSIRO and MIROC-MEDRES models.

The evaluation of the climate projections for the period 2080–2100, demonstrated that a major point of concern is perhaps the inter-model differences, in the spatial distribution and magnitude of the projected changes of the t2m. For instance, CCCma and CSIRO are characterized by higher t2m anomalies over East Antarctica, whereas MIROC-MEDRES and GFDL are dominated by t2m anomalies mainly placed in West Antarctica.

Harmonic analysis reveal that the first harmonic of t2m in the NNR data is characterized by largest seasonal variability over the Weddell and Ross seas, and over the highest topographic features (Dome Fuji and Dome C). Similar analyses for the ERA40 data, however, shows the maximum amplitude over the west Antarctic ice sheet. This may indicate a bias in the ERA40 dataset in regarding the amplitude of the seasonal cycle.

Comparison between the CMIP3 results and the Reanalysis data (Figure 7) clearly demonstrates that the models can satisfactorily simulate the amplitude of the first harmonic, as well as its spatial pattern as seen in the NNR. The CMIP3 results are primarily characterized by the topographic effects over regions such as the East Antarctica Ice Sheet (Figures 6 and 7). Despite showing a good performance over areas of higher seasonal changes, the CMIP3 models show inter-model differences in the amplitude values of the annual harmonic. Larger seasonal variability is identified for CCCma, HadCM3 and MIROC-MEDRES with values as high as 20 °C. The CSIRO model did not exhibit the seasonal variability as predicted by the other models. This feature is tightly linked to the overestimation of the cloud cover as well as is due to weak seasonal changes of precipitation. This overestimation of clouds reduces the annual cycle of temperature in CSIRO and GFDL models (Figure 8).

Calculations of the harmonic analysis based upon GW conditions revealed that global warming affects the annual cycle of Antarctic temperature in different ways over the ocean and the continent (Figure 10). In the interior of the Antarctic continent, there is no substantial seasonal difference between the amplitude of the first harmonic as projected by GW and PD simulations, with values between ± 1 °C. Over the ocean along the ACC, the amplitude of the first harmonic is reduced in all CMIP3 models in the GW interval compared to the PD interval (Figure 10). The CMIP3 models show a large weakening of the annual cycle over the Pacific and Atlantic sectors except for the MIROC-MEDRES. This weakening in the amplitude of the first harmonic is due to higher winter temperatures which is associated with intensified sea ice melting under greenhouse forcing.

Acknowledgements

Support for this research has been provided through Brazilian Antarctic Program (Proj. 550004/2107-6) which is funded by the Brazilian National Research Counsel (CNPq). We acknowledge the modelling groups for making their simulations available for analysis, the Program for Climate Model Diagnosis and Inter-comparison (PCMDI) for collecting and archiving the CMIP3 model output, and the WCRP's Working Group on Coupled Modelling (WGCM) for organizing the model data analysis activity. The WCRP CMIP3 multimodel data set is supported by the Office of Science, US Department of Energy.

References

Aslan Z, cu DO, Kartal S. 1997. Harmonic analysis of precipitation, pressure and temperature over Turkey. *II Nuovo cimento* **20**: 595–605.

Azzali S, Menenti M. 2001. Mapping vegetation-soil-climate complexes in southern Africa using temporal fourier analysis of Noaa-Avhrr Ndvi data. *International Journal of Remote Sensing* **21**: 973–996.

Bjerknes J. 1964. Atlantic air-sea interaction. *Advances in Geophysics* **10**: 1–82.

Bracegirdle TJ, Connelley WM, Turner J. 2008. Antarctic climate change over the twenty first century. *Journal of Geophysical Research* **113**(D3): D03103, DOI:10.1029/2007JD008933.

van den Broeke MR. 1998. The semiannual oscillation and Antarctic climate, part I: Influence on near-surface temperatures (1957-1979). *Antarctic Science* **10**: 175–183.

van den Broeke MR. 2000. On the interpretation of Antarctic temperature trends. *Journal of Climate* **13**: 3885–3889.

van den Broeke MR, Reijmer CH, van As D, van de Wal RSW, Oerlemans J. 2005. Seasonal cycles of antarctic surface energy balance from automatic weather stations. *Annals of Glaciology* **41**: 131–139.

Bromwich DH, Fogt RL. 2004. Strong trends in the skill of the ERA-40 and NCEP-NCAR reanalyses in the high and midlatitudes of the Southern hemisphere, 1958-2001. *Journal of Climate* **17**: 4603–4619.

Cai W, Cowan T. 2007. Trends in southerm hemisphere circulation in IPCC AR4 models over 1950-99: ozone depletion versus Greenhouse forcing. *Journal of Climate*: **20**(4): 681–693.

Cassano JJ, Box JE, Bromwich DH, Li L, Steffen K. 2001. Verification of polar MM5 simulations of Greenland's atmospheric circulation. *Journal of Geophysical Research* **103**: 33867–33890.

Chapman W, Walsh J. 2007. A synthesis of Antarctic temperatures. *Journal of Climate* **20**: 4096–4117.

Connolley WM, Bracegirdle TJ. 2007. An Antarctic assessment of IPCC AR4 coupled models. *Geophysical Research Letters* **34**: L22505, DOI:10.1029/2007GL031648.

Cressman GP. 1959. An operational objective analysis system. *Monthly Weather Review* **87**: 367–374.

Delworth TL, Broccoli AJ, Rosati A, Stouffer RJ, Balaji V, Beesley JA, Cooke WF, Dixon KW, Dunne J, Dunne KA, Durachta JW, Findell KL, Ginoux P, Gnanadesikan A, Gordon CT, Griffies SM, Gudgel R, Harrison MJ, Held IM, Hemler RS, Horowitz LW, Klein SA, Knutson TR, Kushner PJ, Langenhorst AR, Lee H-C, Lin S-J, Lu J, Malyshev SL, Milly PCD, Ramaswamy V, Russell J, Schwarzkopf MD, Shevliakova E, Sirutis JJ, Spelman MJ, Stern WF, Winton M, Wittenberg AT, Wyman B, Zeng F, Zhang R, Part I. 2006. GFDL's CM2 global coupled climate models. Formulation and simulation characteristics. *Journal of Climate* **19**(5): 643–674.

Flato GM, Boer G. 2001. Warming asymmetry in climate change simulations. *Geophysical Research Letters* **28**: 195–198.

Fyfe JC, Saenko OA, Zickfeld K, Eby M, Weaver AJ. 2007. The role of poleward intensifying winds on Southern Ocean warming. *Journal of Climate* **20**: 5391–5400.

Gordon HB, Rotstayn LD, McGregor JL, Dix MR, Kowalczyk EA, O'Farrell SP, Waterman LJ, Hirst CA, Wilson SG, Collier MA, Watterson IG, Elliott TI. 2002. The CSIRO Mk3 Climate System Model [Electronic publication]. Aspendale: CSIRO Atmospheric Research. Technical Report 60, CSIRO Atmospheric Research.

Hasumi H, Emori S. 2004. K-1 coupled GCM (MIROC) description. Technical report, Centre for Climate and Sustainable Research (CCSR), University of Tokyo.

Hines KM, Bromwich DH, Marshall GJ. 2000. Artificial surface pressure trends in the NCEPNCAR reanalysis over the Southern Ocean and Antarctica. *Journal of Climate* **13**: 3940–3952.

Holland MM, Raphael MN. 2006. Twentieth century simulation of the southern hemisphere climate in coupled models. Part II: sea ice

conditions and variability. *Climate Dynamics* **26**(2–3): 229–245, DOI:10.1007/s00382-005-0087-3.

Jakubauskas ME, Legates D, Kastens JH. 2001. Harmonic analysis of time-series AVHRR NDVI data. *Photogrammetric Engineering and Remote Sensing* **67**: 461–470.

Justino F, Peltier WR. 2008. Climate anomalies induced by the Arctic and Antarctic oscillations: glacial maximum and present-day perspectives. *Journal of Climate* **21**: 459–475.

Justino F, Timmermann A, Merkel U, Peltier W. 2006. An initial intercomparison of atmospheric and oceanic climatology for the ICE-5G and ICE-4G models of LGM paleotopography. *Journal of Climate* **19**: 3–14.

Kalnay E, Kanamitsu M, Kistler R, Collins W, Deaven D, Gandin L, Iredell M, Saha S, White G, Woolen J, Zhu Y, Chelliah M, Ebisuzaki W, Higgins W, Janowiak J, Mo KC, Ropelewski C, Wang J, Leetma A, Reynolds R, Jenne R, Joseph D. 1996. The NCEP-NCAR 40 Year reanalysis project. *Bulletin of the American Society* **77**: 437–471.

King JC. 1994. Recent climate variability in the vicinity of the Antarctic Peninsula. *International Journal of Climatology* **14**(4): 357–369.

Kushner PJ, Held IM, Delworth TL. 2001. Atmospheric circulation response to global warming. *Journal of Climate* **14**: 2238–2249.

Lefebvre W, Goosse H, Timmermann R, Fichefet T. 2004. Influence of the southern annular mode on the sea ice-ocean system. *Journal of Geophysical Research* **109**: DOI:10.1029/2004JC002403.

Marshall GJ, King JC. 1998. Southern hemisphere circulation anomalies associated with extreme antarctic peninsula winter temperatures. *Geophysical Research Letters* **25**: 2437–2440.

Meehl G. 1991. A reexamination of the mechanism of the semiannual oscillation in the southern hemisphere. *Journal of Climate* **4**(9): 911–926, DOI: 10.1175/1520-0442(1991)004<0911:AROTMO>2.0.CO;2.

Meehl GA, Washington WM, Santer BD, Collins WD, Arblaster JM, Hu A, Lawrence DM, Teng H, Buja LE, Strand WG. 2006. Climate change projections for the twenty-first century and climate change commitment in the ccsm3. *Journal of Climate* **19**(11): 2121–2632.

Miller RL, Schmidt GA, Shindell DT. 2006. Forced annular variations in the 20th century Intergovernmental Panel on Climate Change Fourth Assessment Report models. *Journal of Geophysical Research* **111**: D18101, DOI:10.1029/2005JD006323.

Monaghan AJ, Bromwich DH. 2008. Advances in describing recent Antarctic climate variability. *Bulletin of the American Meteorological Society* **89**: 1295–1306.

Monaghan AJ, Bromwich D, Schneider D. 2008. 20th century Antarctic air temperature and snowfall simulations by IPCC climate models. *Geophysical Research Letters* **35**: L07502, DOI: 10.1029/2007GL032630.

Phipps SJ. 2006. On Long-Term Climate Studies Using a Coupled General Circulation Model. Ph.D. thesis, University of Tasmania.

Pope VD, Gallani M, Rowntree PR, Stratton RA. 2000. The impact of new physical parametrizations in the Hadley Centre climate model – HadAM3. *Climate Dynamics* **16**: 123–146.

Raphael MN, Holland MM. 2006. Twentieth century simulation of the southern hemisphere climate in coupled models. Part 1: large scale circulation variability. *Climate Dynamics* **26**: DOI:10.1007/s00382-005-0082-8.

Rind D. 1987. Components of the ice age circulation. *Journal of Geophysical Research* **92**: 4241–4281.

Russell JL, Stouffer RJ, Dixon KW. 2006. Intercomparison of the Southern ocean circulations in IPCC coupled model control simulations. *Journal of Climate* **19**: 4560–4574.

Turner J, Connolley WM, Lachlan-Cope TA, Marshall GJ. 2006. The performance of the Hadley Centre Climate Model (HadCM3) in high southern latitude. *International Journal of Climatology* **26**: 91–112, DOI:10.1002/joc.1260.

van Loon H. 1967. The Half-Yearly Oscillations in Middle and High Southern Latitudes and the Coreless Winter. *Journal of the Atmospheric Sciences* **24**: 472–486.

Vaughan DG, Bamber JL, Giovinetto M, Russell J, Cooper APR. 1999. Reassessment of net surface mass balance in Antarctica. *Journal of Climate* **12**: 933–946.

Warren SG. 1996. Antarctica. *Encyclopedia of Weather and Climate*. Oxford University Press: Cambridge UK; 1: 32–39.

Wilks DS. 1995. *Statistical Methods in the Atmospheric Sciences: An Introduction*. Academic Press: San Diego.

Yuan X, Li C. 2008. Climate modes in southern high latitudes and their impacts on antarctic sea ice. *Journal of Geophysical Research* **113**(C6):, DOI:10.1029/2006JC004067.

Yuan XJ, Martinson DG. 2000. Antarctic sea ice extent variability and its global connectivity. *Journal of Climate* **13**: 1697–1717.

